International Journal of Biological Macromolecules 220 (2022) 1523–1531

Contents lists available at ScienceDirect

International Journal of Biological Macromolecules

journal homepage: www.elsevier.com/locate/ijbiomac

Serum albumin/hyaluronic acid nanoconjugate: Evaluation of concentration-dependent structural changes to form an efficient drug carrier particle

Norbert Varga, László Seres, Nikolett Alexandra Kovács, Árpád Turcsányi, Ádám Juhász, Edit Csapó *

MTA-SZTE Lendület "Momentum" Noble Metal Nanostructures Research Group, University of Szeged, H-6720 Rerrich B. sqr. 1, Szeged, Hungary
Interdisciplinary Excellence Center, Department of Physical Chemistry and Materials Science, University of Szeged, H-6720 Rerrich B. sqr. 1, Szeged, Hungary

ARTICLE INFO

Keywords:
Human serum albumin
Hyaluronic acid
Nanoconjugates

ABSTRACT

In actual work we clearly highlight in the first time the experimental factors (dominantly the concentration of the macromolecule components) influencing the formation of human serum albumin/hyaluronic acid (HSA/HyA) complex carrier particles which is not available in the literature despite the several published articles. We have shown that the charge compensation process of the oppositely charged macromolecules results in the formation of drug carrier particles (d ~ 200–350 nm), where the size, size distribution and structure can be largely controlled by changing the concentration of the macromolecule components and the experimental conditions (pH, reaction time, presence of inert salt *etc.*). Moreover, we firstly demonstrate the encapsulation capability of this optimized HSA/HyA carrier particles - which possess dominantly hydrophilic character - using vitamin D3 (D3) as a model compound having hydrophobic property, where the kinetic properties of the dissolution were studied as well.

1. Introduction

The delivery of the active ingredient molecule to the appropriate point in the human body, as well as the maintenance of the necessary therapeutic dose for a long time are significant challenges in the development of an advanced and effective medicine. Different colloidal drug delivery systems can be successfully applied to solve these problems, because their physical, chemical, and pharmacokinetic parameters can be optimized by the chemical composition and the structure of the carrier [1,2].

The use of polysaccharides (*e.g.* hyaluronic acid (HyA), chitosan (Chit) *etc.*) and serum proteins (*e.g.* mainly bovine serum albumin (BSA)) as nanosized drug carriers are well-known in the literature [3]. To reach effective carrier particles with narrow size distribution and higher encapsulation efficiency, the structure of the mentioned macromolecules needs to be modified; generally, it is available for the application of cross-linkers [4,5] or modification of the structure [6] by chemical ways. On the other hand, the structure-dependent properties of the carrier can be enhanced by the design of substrates with mixed composition, which is most easily achieved by charge compensation of the components [7,8]. Thanks to the excellent biocompatibility and biodegradability, the HyA can be preferable used in nanomedicine [9]. For HyA-based carrier particles, the charge compensation-based preparation technique plays increasingly important role, where the formation of particles, and thus hydrophobicity of the macromolecule chains, can be achieved by the electrostatic interaction between the negatively charged HyA and the other component having positive charge. As cationic agents, various surfactants (such as cetrimonium bromide [10]), polymers/polyelectrolytes (Chit) [11], polyarginine [12] *etc.*) and proteins (*e.g.* (BSA) [13,14], human serum albumin (HSA) [15]) can be used. For human therapy, the application of HSA is more preferred. The HSA can bind both the hydrophobic [16,17] and hydrophilic [18] drug molecules as well. The formation of HSA/HyA conjugates can be achieved by desolvation [19], precipitation [20] or solvent displacement [21] techniques. It is important to note, that the most synthesis techniques for production of HSA/HyA complex carrier particles require desolvation (*e.g.* dichloromethane, ethanol, acetone) or cross-linking (*e.g.* glutaraldehyde) agents, which presence in the systems is disadvantageous in terms

* Corresponding author at: MTA-SZTE Lendület "Momentum" Noble Metal Nanostructures Research Group, University of Szeged, H-6720 Rerrich B. sqr. 1, Szeged, Hungary.
E-mail address: juhaszne.csapo.edit@med.u-szeged.hu (E. Csapó).

https://doi.org/10.1016/j.ijbiomac.2022.09.125
Received 22 July 2022; Received in revised form 9 September 2022; Accepted 14 September 2022
Available online 16 September 2022

of biomedical applications [22]. To eliminate them, the simple electrostatic complexation can be perfectly applied, where the particles are created by neutralizing the anionic HyA polymer chains with proteins having dominantly positive charge in one step.

We successfully presented previously the fabrication protocol as well as the detailed structural characterization of HyA/Chit [23] and BSA/HyA [24] complex carriers. The combination of the two polysaccharides and polysaccharide with BSA resulted in controlled preparation protocol, well-defined particle size, narrow size distribution and controlled encapsulation capacity for ibuprofen (IBU) as model drug molecule. In latter case we clearly confirmed that by replacing BSA with HSA [25], the drug release is measurably different, despite the two proteins having almost identical size and structure. We have firstly demonstrated that under the same conditions (concentration, pH), different charge ratios can be identified, which have a significant effect on the structure of the complex substrates formed by charge complexation, and which requires detailed investigation of the interactions between the HyA and HSA using a range of physicochemical measurement techniques. It is important to note that the effect of pH on the fabrication possibilities of the HSA/HyA systems is mainly investigated in the literature, but there is only a little information on the effect of the change of the determinative experimental parameters on size, structure, and morphology of the carrier particles. In addition, measurable less information about the HSA-based carriers is available, as the much cheaper BSA derivative is used [26,27].

Based on this observation, in this article we demonstrate in the first time the experimental factors (mainly the concentration) influencing the formation of HSA/HyA complex carrier particles which is not available in the literature despite the several reported articles. Namely, the electrostatic interactions between the mentioned protein and polysaccharide have been investigated in detail and the structural changes of the HSA during fabrication were also evaluated. Moreover, we firstly present the encapsulation capability of this optimized HSA/HyA carrier particles for vitamin D3 (D3) as a model compound having hydrophobic property, where the kinetic properties of the dissolution were studied as well.

2. Materials and methods

2.1. Materials

Hyaluronic acid sodium salt (HyA, 1.5–1.8·10^6 Da), human serum albumin (HSA, ~67 kDa, fatty acid-free (≤0.1 %)), cholecalciferol (Vitamin D3 (abbrev: D3), $C_{27}H_{44}O$; ≥98 %) and sodium dodecyl sulphate (SDS; $CH_3(CH_2)_{11}OSO_3Na$; ≥99 %) were obtained from Sigma-Aldrich. Sodium acetate 3-hydrate ($CH_3COONa{\cdot}3H_2O$; ≥99 %) and acetic acid (CH_3COOH; ≥99 %) were purchased from VWR International. Sodium phosphate dibasic dodecahydrate ($Na_2HPO_4 \times 12H_2O$; ≥99 %), sodium phosphate monobasic monohydrate ($NaH_2PO_4 \times H_2O$; ≥99 %), sodium chloride (NaCl; ≥99 %) and ethanol (CH_3CH_2OH; ≥99 %) were obtained from Molar Chemicals. Highly purified water was obtained by deionization and filtration with a Millipore purification apparatus (18.2 MΩ·cm at 25 °C). All the solvents and reagents used for preparations were analytical grade and further purifications were not applied.

2.2. Methods

2.2.1. Synthesis of the drug-free and D3-loaded HSA/HyA nanosized particles

The HSA/HyA systems were prepared in acetate buffer (pH = 4.50) by charge neutralization method, where the formation of the carrier particles was studied under different initial conditions: m_{HSA}/m_{HyA} = 0.21–5.00 ratio, c_{HyA} = 0.05–0.20 mg/mL, c_{NaCl} = 0–0.06 M, 10 μL/0–180 s dosing speed and T = 10–40 °C. Before preparation of the particles, the 1 mg/mL HyA stock solution was stirred for 30 min under 300 rpm and stored for 24 h at 10 °C. During the preparation process, 20 mg/mL HSA solution was added dropwise (10–40 μL) into the 20 mL diluted HyA solutions under 500 rpm magnetic stirring. After the mixing of the solutions, the samples were stirred for at least 1 h before further use. At the D3-loaded HSA/HyA (D3/HSA/HyA) particles, the D3 was dissolved in 50 μL ethanol (c_{D3} = 5, 10 and 20 mg/mL), which were added 300–300 μL 6.67 mg/mL HSA solutions. The mixtures were dropped in 20 mL, 0.05 mg/mL HyA solutions under 10 μL/2 min dosing speed. The HSA/HyA and D3/HSA/HyA particles were centrifugated (12,000 rpm, 15 min) and freeze-dried (Christ Alpha 1–2 LD plus), and the solid samples were stored at −20 °C.

2.2.2. Rheology

The apparent viscosity curves of the HSA/HyA systems were determined by Anton Paar Physica MCR 301 Rheometer (Anton Paar, GmbH, Germany) at 25 ± 0.1 °C and 300 1/s shear rate. The measuring system was equipped with concentric cylinder geometry (CC27-SN12793). For the determination of the rheological properties, the HSA (20 mg/mL) and HyA (0.05; 0.10; 0.15; 0.20 mg/mL) solutions were prepared in pH = 4.5 acetate buffer. HSA solution was added dropwise in the 19 mL HyA solution with 10–40 μL/3 min dosing speed. The effect of dilution of HyA was also investigated (Figs. S1, S2).

2.2.3. Charge titration

The charge titration curves of HSA/HyA systems were determined by a Mütek Particle Charge Detector PCD-04 model. Under the measurements, the 19 mL HyA solutions were titrated dropwise by 20 mg/mL HSA solution at 25 °C and the streaming potential values (mV) were registered. During the characterization, 0.05–0.20 mg/mL HyA concentrations and acetate buffers (pH = 3.6 and 4.5) were used. Analysis of the obtained results was performed by using the modified version of the sigmoidal Boltzmann equation [23].

2.2.4. Circular dichroism spectroscopy

CD curves were recorded by a Jasco J-1100 CD spectrometer at 25 ± 1 °C and 100 nm/min scanning speed. The spectra of the HSA and HSA/HyA systems were determined in the middle UV-region (200–300 nm) under continuous (3 L/min) N_2 flow, where the light source was a water-cooled, high-energy xenon lamp (450 W). The raw data (average three scans per samples) was converted into mean residue ellipticity (MRE) (Eq. (1)), and the ratio of the α-helix content was calculated from the (Eq. (2)).

$$\mathrm{MRE}_{208} = \frac{\mathrm{observedCD(mdeg)}}{10 C_p n l} \tag{1}$$

$$\alpha - \mathrm{helix}\ (\%) = \frac{-\mathrm{MRE}_{208} - 4000}{33000 - 4000} \times 100 \tag{2}$$

where the C_p is the molar concentration of the protein, n is the number of amino acid residues, and l is the pathlength of the cuvette (1 cm in our case).

2.2.5. Thermoanalytical studies

Thermogravimetric (TG) and the Differential scanning calorimetry (DSC) curves of the solid samples were determined by Mettler-Toledo TGA/SDTA 851e Instrument and Mettler Toledo DSC822e, where the observed temperature ranges were 25–700 °C (TG) and 25–500 °C (DSC), while the heating rate was 5 °C/min.

2.2.6. Characterization of the particles

The hydrodynamic diameter, size distribution and zeta potential (ζ-potential) values were determined by a HORIBA SZ-100 NanoParticle Analyzer (Retsch Technology GmbH), using semiconductor laser (λ = 532 nm, 10 mW) as light source and photomultiplier tubes (PMT) as detector at 90° scattering angle. The transmission electronmicroscopic

(TEM) images were recorded by a Jeol JEM-1400plus equipment (Japan) at 120 keV accelerating. A Precision Bench Turbidity Meter LP2000 (Hanna Ins.) was used for turbidity measurements.

For the determination of the encapsulation efficiency (EE%) and the drug loading (DL%), the lyophilized solid D3/HSA/HyA samples were redispersed in ethanol using ultrasonic bath at 25 °C. After 10 min sonication, the dispersions were stirred for 2 h and centrifugated (10,000 rpm, 10 min). The absorbance spectra of the supernatants of the redispersed D3/HSA/HyA samples were registered in 200–500 nm wavelength range by Shimadzu UV-1800 UV–Vis spectrophotometer. The degree of the encapsulation of the model hydrophobic drug was determined from the calibration curves using the measured absorbance at λ = 270 nm in ethanol (Fig. S3). The EE% and DL% values were defined by Eqs. (3)–(4).

$$EE\% = \frac{\text{encapsulation mass of drug}}{\text{total mass of drug}} \times 100 \quad (3)$$

$$DL\% = \frac{\text{encapsulation mass of drug}}{\text{total mass of nanoparticles}} \times 100 \quad (4)$$

2.2.7. *In vitro release studies*

The *in vitro* release of the bulk (solid powder of D3), the dissolved (D3 solution in same amount) and the encapsulated D3 from the carrier were carried out by UV–Vis spectrophotometer, where the changes of the concentration of the active compound were determined by calibration curves at λ = 267 nm (Fig. S4). The dissolution was studied at 37 °C in PBS buffer (pH = 7.4, NaCl 0.9 %) for 420 min. To facilitate the better solubility of the dissolved model drug molecules, 0.5 % sodium dodecyl sulphate (SDS) was added into the media [28]. The D3 samples with 5 mL of SDS/PBS medium were placed in the semipermeable cellulose membrane (M_w cut-off = 14,000; Sigma-Aldrich), which were inserted into 35 mL dissolution phase. The acquired results were fitted by QtiPlot 0.9.8.9 svn 2288 program with different kinetic models (zero order, first order, Korsmeyer–Peppas, Peppas-Sahlin, Higuchi, Hopfenberg and Weibull equation) [5,29,30].

3. Results

3.1. *Rheology and charge titration studies*

In our previous publication, we interpreted the effect of the pH to the preparation possibilities of BSA/HyA systems, and the optimal value was determined at pH = 4.5 [24]. Using this optimized pH = 4.5 (in acetate buffer medium), where the HyA and HSA possess opposite surface charges (HyA: pK_a ~ 3–4 [31]; HSA: isoelectric point (pI) pI = 4.7 [32]), the effect of the HyA concentration to the HSA/HyA system was examined by rheology and charge titration methods (Fig. 1A, B). The apparent viscosity curves as a function of the m_{HSA}/m_{HyA} ratio show breaking points (Fig. 1A); the detected breaking points are observed at increasingly higher m_{HSA}/m_{HyA} mass ratios as the concentration of HyA increases. This systematic change can be detected for the charge titration studies as well. Based on the fitting of the modified sigmoidal Boltzmann equation, the inflection point is continuously shifted with increasing HyA concentration (Fig. 1B). In contrast to the BSA/HyA systems, which have a neutralization point at m_{BSA}/m_{HyA} = 5.05 at pH = 4.5 under same concentration and buffer [24], the streaming potential values for HSA tend asymptotically to 0 mV, but neutralization is not occurred. This observation confirms our finding that two proteins interact differently with HyA at the same pH and concentration, which may result from their different pI (pI_{BSA} = 5.1; pI_{HSA} = 4.7) [25].

These measurements were also performed at pH = 3.6 acetate buffer, and similar effects are observed for the shift of the inflection point (Fig. S5), however, as expected, the neutralization is observed in this case due to the lower pH. If we assume purely electrostatic interactions between the two macromolecules, the inflection points (Fig. 1C) should appear at the same mass ratio values without any shift. These results may indicate the existence of hydrophobic interactions as well in the studied protein/polymer system. In this regard, it is essential to consider the concentrations of the components for characterization of these complex conjugates, because significant differences can be obtained for the system-specific parameters.

3.2. *Effect of pH and HyA concentration on the drug-free HSA/HyA carrier particles*

After rheology and charge titration experiments, the formation of HSA/HyA particles through interactions between macromolecules and their characteristic structural properties (size, size distribution, ζ-potential *etc.*) were studied at different pH and wide m_{HSA}/m_{HyA} mass ratio ranges by dynamic light scattering (DLS). Figs. 2 and S6 show that nearly constant particle size can be achieved at lower HSA to HyA mass ratios (~200 nm (pH = 3.6), ~205 nm (pH = 4.0) and ~285 nm (pH = 4.5) up to m_{HSA}/m_{HyA} = 2). After a significant increase in the hydrodynamic diameter, the aggregation of the particles is appeared m_{HSA}/m_{HyA} = 1.89, 2.74 and 4.21 at pH = 3.6, 4.0 and 4.5, respectively, which occur very close to the inflection point of the curves. The ζ-potential values (analogous to the streaming potential) are constantly changing, especially near the inflection point, where the particles have less and less stability. In Fig. 2, it also can be observed that the ζ-potential at HSA excess (for the last few points of the curves) is close to +30 mV (pH =

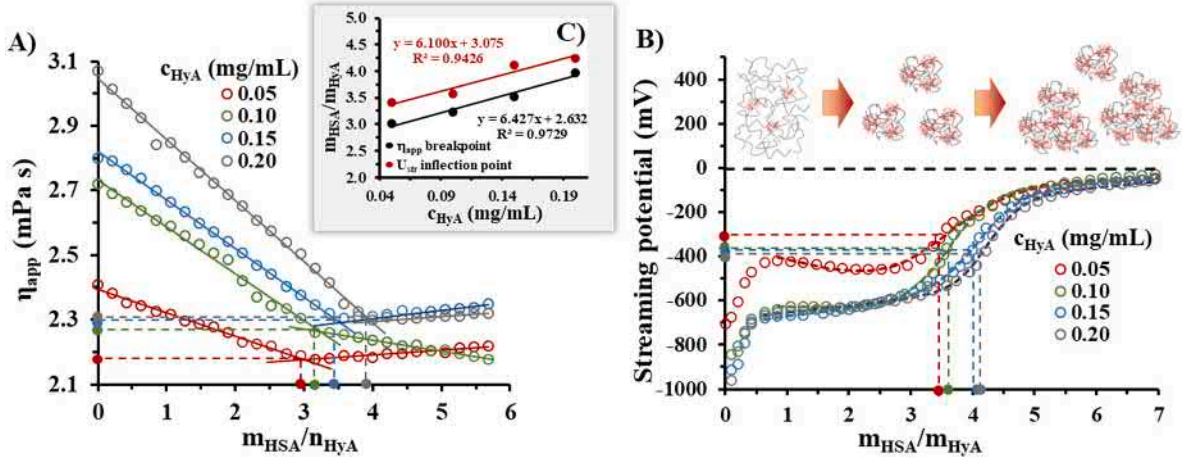

Fig. 1. Change of the (A) apparent viscosity and (B) streaming potential of HSA/HyA system at different initial HyA concentration values (pH = 4.5 acetate buffer; V_{HyA} = 19 mL; c_{HSA} = 20 mg/mL). (C) The detected breaking points and inflection points as a function of HyA concentration.

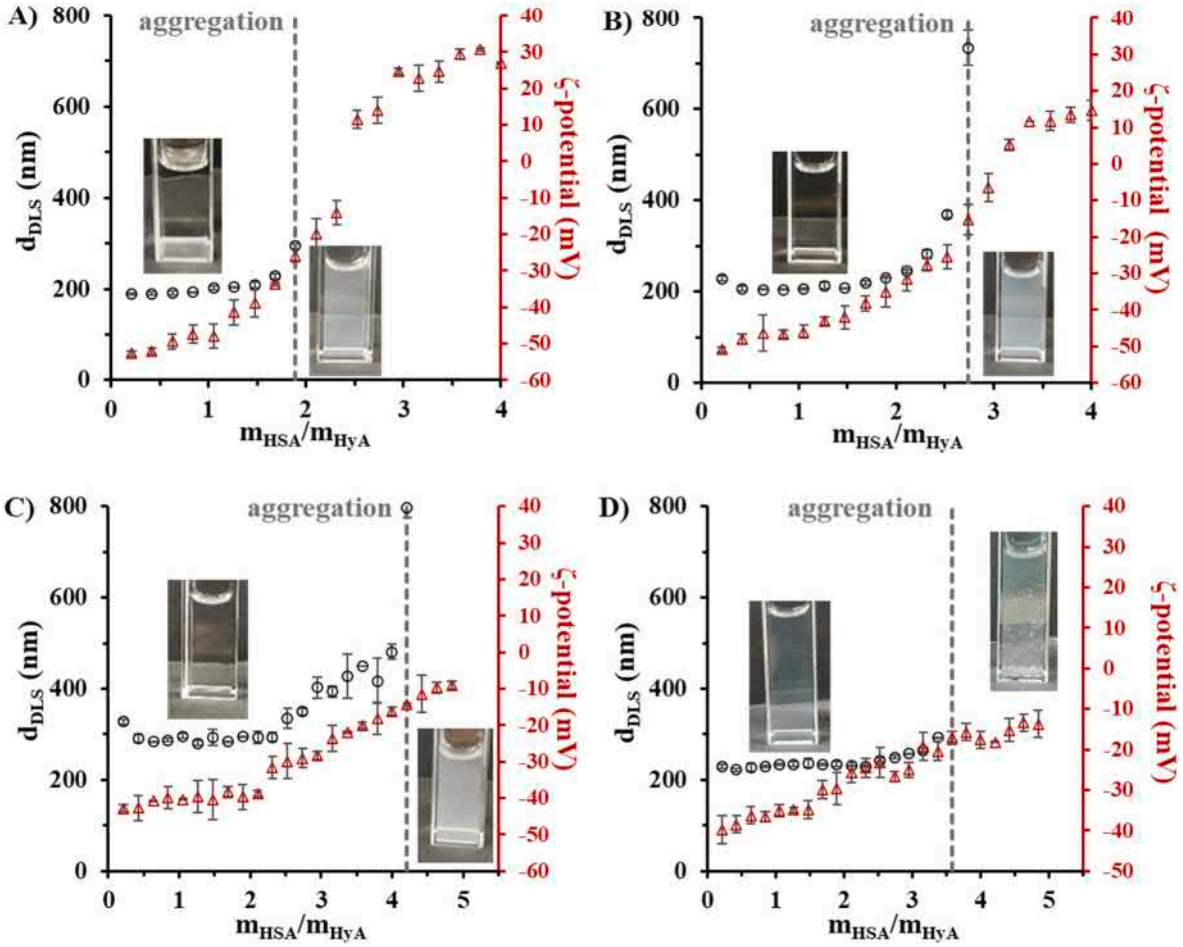

Fig. 2. The hydrodynamic diameter (○, left y-axis) and the ζ-potential (△, right y-axis) of the HSA/HyA conjugates at (A) pH = 3.6, (B) pH = 4.0, (C) pH = 4.5 (c_{HyA} = 0.1 mg/mL, V_{HyA} = 20 mL, c_{HSA} = 20 mg/mL) and (D) 0.05 mg/mL HyA concentration (pH = 4.5 acetate buffer; V_{HyA} = 20 mL; c_{HSA} = 20 mg/mL) (The measuring data with the appropriate errors are seen in Tables S1, S2). (For interpretation of the references to color in this figure legend, the reader is referred to the web version of this article.)

3.6) (Fig. 2A), +10 mV (pH = 4.0) (Fig. 2B) and 0 mV (pH = 4.5) (Fig. 2C). Considering the pH of the samples, this change can be explained by the decreasing of the positive charge of the HSA with increasing pH.

To confirm the DLS and ζ-potential results, turbidimetric studies were performed, where the turbidity of the dispersion was determined under the same experimental conditions (Fig. S7A). Initially, the turbidity is increased due to the continuous formation of the particles, but after the aggregation point, the large particles are deposited, which is resulted the decreasing of the values. From the maximum values of the turbidity (aggregation point), we obtained the protein to polysaccharide mass ratios with a very good agreement to the light scattering results. Based on the previously mentioned effect of the HyA concentration, we also determined the turbidity, hydrodynamic diameter, and ζ-potential at 0.05 mg/mL HyA in pH = 4.5 acetate buffer as well (Figs. 2D, S7B). The Fig. 2C, D show that much smaller size can be detected in wide mass ratio range, when higher concentrations of HyA is applied (~240 nm for 0.05 mg/mL HyA, ~285 nm for 0.10 mg/mL HyA). This observation also proves the dominant effect of HyA concentration on the hydrodynamic diameter. In line with previous results, the HSA/HyA particles are aggregated at higher mass ratios by the increasing of the presence of the HyA macromolecule, which is also confirmed by turbidimetric measurements (Fig. S7B). Examining the zeta potential values, their continuous increase can be observed due to the addition of HSA.

Based on the previous measurements at different pH, the preparation of stable particles is possible at m_{HSA}/m_{HyA} = 1 ratio, thus, the characterization of these particles was performed using 1:1 mass ratio with different HyA concentrations (Fig. 3). From the determined size distribution curves at pH = 4.5, it can be clearly seen that the maximum of the peak shifts to the larger hydrodynamic diameters by increasing the amount of the polysaccharide (Fig. 3A). Moreover, considering the change of the size distribution, formation of a much more polydisperse system can be observed. The determined average particle size is changed from ~240 nm (0.05 mg/mL HyA) to ~405 nm (0.20 mg/mL HyA), while the ζ-potential has a systematically lower negative value from ~−35 mV (0.05 mg/mL HyA) to ~−46 mV (0.20 mg/mL HyA) (Fig. 3B). As the lower polydispersity and hydrodynamic diameter (below 300 nm for blood brain barrier) are the favourable for the drug carriers, thus below 0.1 mg/mL HyA concentration are optimal to produce these HSA/HyA-based systems.

3.3. *Effect of the experimental conditions on the drug-free HSA/HyA NPs*

The effect of further experimental conditions like the dosing speed during the components mixing, inert salt (NaCl), HSA concentration and the temperature on the prepared HSA/HyA systems have been studied at pH = 4.5 using 0.05 mg/mL HyA (Fig. 4). In the knowledge of the concentration dependence (Fig. 2), the experiments were performed with 2:1 HSA:HyA mass ratio, because the dispersion is still stable and enough proteins can interact with the polysaccharide. Firstly, we characterized the role of the dosing speed on the hydrodynamic diameters and ζ-potential (Fig. 4A). Fig. 4A shows, significantly larger particle size

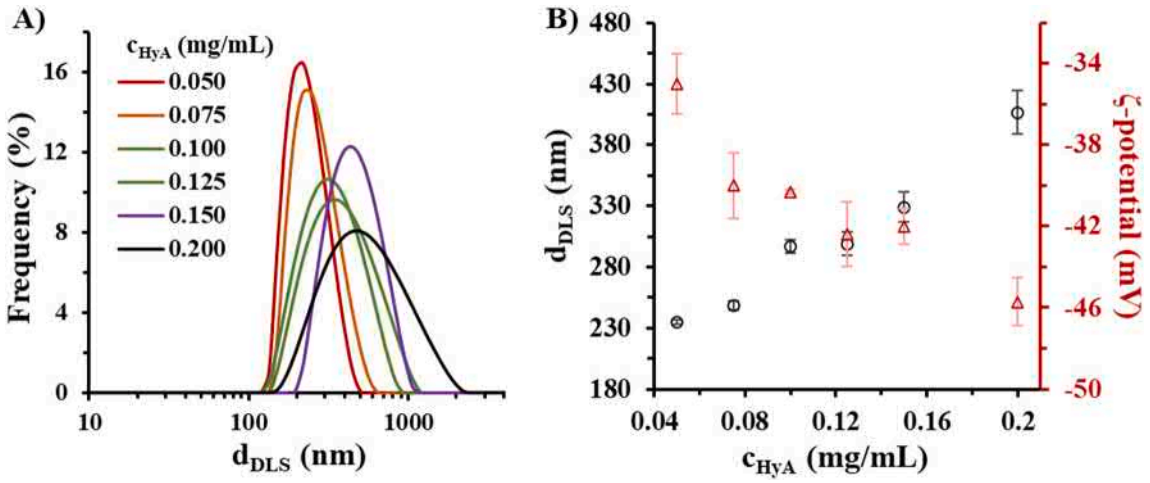

Fig. 3. (A) Representative DLS curves and (B) hydrodynamic diameter (○, left y-axis) and the ζ-potential (△, right y-axis) values of HSA/HyA particles at different HyA concentration (pH = 4.5 acetate buffer, $m_{HSA}/m_{HyA} = 1$, $V_{HyA} = 20$ mL, $c_{HSA} = 20$ mg/mL) (The measuring data with the appropriate errors are presented in Table S3). (For interpretation of the references to color in this figure legend, the reader is referred to the web version of this article.)

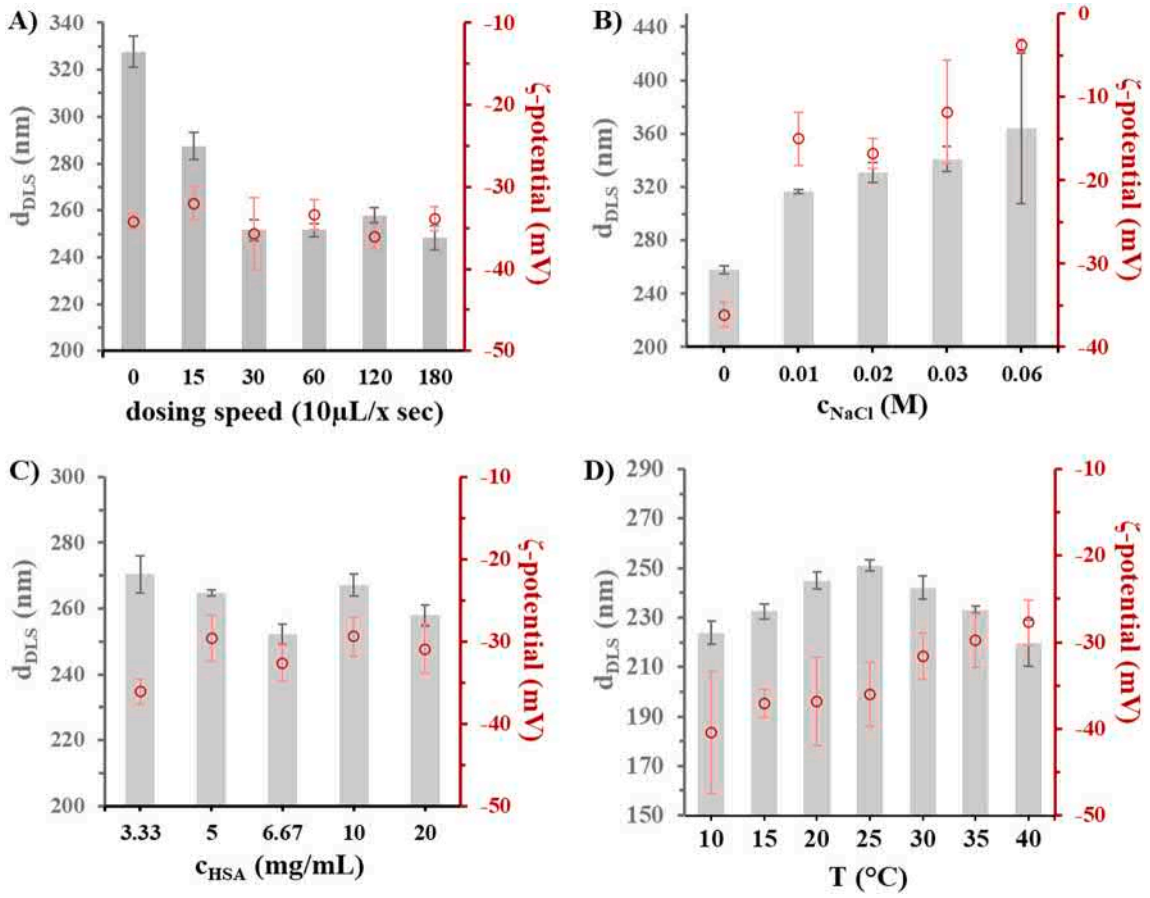

Fig. 4. The hydrodynamic diameter (grey column, left y-axis) and the ζ-potential (○, right y-axis) of the HSA/HyA particles at different (A) dosing speed, (B) NaCl concentration, (C) HSA concentration and (D) temperature (pH = 4.5 acetate buffer, $m_{HSA}/m_{HyA} = 2$, $c_{HyA} = 0.05$ mg/mL, $V_{HyA} = 20$ mL) (The measuring data with the appropriate errors are presented in Table S4). (For interpretation of the references to color in this figure legend, the reader is referred to the web version of this article.)

can be produced with lower dosing steps ($d_{DLS} \sim 328$ nm and $d_{DLS} \sim 287$ nm at 0 s/10 μL and 15 s/10 μL, respectively), than 30s/10 μL ($d_{DLS} \sim 252$ nm). However, the further increase of the duration does not cause a significant change in either the hydrodynamic diameter or the zeta potential ($\zeta_{average} = -34 \pm 2$ mV). Based on these, it can be stated that the use of higher dosing speed is optimal to produce HSA/HyA particles. The effect of the inert salt on electrostatic stability was studied using NaCl ($c_{NaCl} = 0$–0.06 M) (Fig. 4B). As it can be seen on Fig. 4B, the size and the ζ-potential constantly increase from ~258 nm and ~−36 mV (0 M NaCl) to ~364 nm and ~−3.8 mV (0.06 M NaCl). This change can be

explained that the appearance of an inert salt in the dispersion reduces the electrostatic repulsion between the particles, because the conjugates charge can be covered by the ions with opposite charge to the adducts. It appears significant increase in particle size at lower ionic strength values, while the dispersion destabilizes and aggregates at higher salt concentrations. The effect of the concentration of HSA stock solution was also examined (Fig. 4C). Based on the results, significant change is not observed during these studies, and we obtained that this parameter does not play an influential role in the formation of carrier conjugates only the mass ratio of the macromolecules. For the temperature dependence, 10–40 °C interval was used due to avoid protein precipitation. Fig. 4D presents that the hydrodynamic diameter follows a maximum curve, and the largest particle size can be achieved at 25 °C (251 ± 2 nm). At higher temperatures, the decrease in size can be explained by denaturation of the protein, because much less protein is able to interact with HyA. The small particle sizes at lower temperatures can be explained with so-called "cold denaturation" [33]. This phenomenon starts in the temperature range above the freezing point of water, which is due to fact that the process of the unfolding of globular proteins has a high positive heat-capacity, mainly due to hydrophobic interactions. In this sense, it is conceivable that the effect of the initial stage of this process can be observed in the change of the particle size. Contrast to the particle size, the zeta potential shows a steady increase, thus, the HSA/HyA system has lower electrostatic stability by the increasing of the temperature.

3.4. Morphology and structural characterizations of the optimized HSA/HyA particles

Based on the results of the previous section, we obtained a preparation protocol using the following parameters: $m_{HSA}/m_{HyA} = 2$; $c_{HSA} =$ 20 mg/mL, $V_{HSA} = 100$ μL, $c_{HyA} = 0.05$ mg/mL, $V_{HyA} = 20$ mL, 10 μL/120 s HSA dosing speed, $T = 25$ °C, pH = 4.5 acetate buffer medium. The morphology, size, and the size distribution (number average) of the prepared HSA/HyA NPs were characterized by TEM (Fig. 5). The TEM images confirmed the conjugates having ~232 nm average diameter. This value is close to the DLS results (~251 nm), the difference can be explained by the hydrodynamic diameter. The interaction between the two macromolecules and the degradation temperature (T_d) of the prepared conjugate were determined by thermoanalytical measurements (Figs. 6A, S8). According to the DSC curves (Fig. 6A), the T_d value of the HSA is 205 °C. The exothermic peak of the HyA and the endothermic peak of HSA are not detected for HSA/HyA NPs, which indicates the absence of the free macromolecules and the presence of the electrostatic and hydrophobic interactions. Above 325 °C, the heating flow continuously increases, as it is seen for pure HSA as well. This is presumably caused by the large amount of protein interacting in the conjugate. The sample was also studied by TG measurements, where the determined T_d of the HSA/HyA particles is 199 °C, lower than HyA (223 °C) and HSA (209 °C) (Fig. S8). The structure of the HSA was followed by CD spectroscopy (Figs. 6B, S9). Fig. 6B shows that the calculated α-helix content of the HSA is 67.3 % at pH = 4.5 (Eq. (1), Eq. (2)). When the polysaccharide appears, it causes a significant change in the secondary structure of the protein, and the α-helix content is decreased to 28.2 %. The CD curves of the HSA and the conjugate were fitted by Reed model [34] and the results are pointed out the β-sheet content is increased (29.4 % (HSA); 60.7 % (HSA/HyA)) in addition to the change in α-helix (Table S5). The effect of the presence of HyA on the HSA structure clearly proves the formation of electrostatic and hydrophobic interactions which is resulted, the HyA polymer chains does not allow the protein to unfold to the extent, as it can do in the solvated form in the buffer. If the pH is higher (pH = 7.4, Fig. 6C), than the isoelectric point of HSA (pI = 4.7 [32]), the HSA structure are shown less change with the addition of HyA (48.3 % (HSA); 55.8 % (HSA/HyA)), which indicates a decrease of the electrostatic interaction. Further studies were also performed at pH = 3.6 (Fig. S9A, Table S6). In this case, the HSA/HyA 1:1 mass ratio was used to avoid the aggregation and it was found that the HSA excess (from 1:1 to 2:1) does not significantly change the run of the CD curves. In Fig. S9B, similar change is observed at pH = 3.6 and 4.5, which is confirmed, the decreasing of the pH (and the charge of the HyA in this range) does not have dominant effect on the protein structure.

3.5. Characterization of D3-loaded HSA/HyA NPs

During the study of the applicability of the HSA/HyA conjugate as a drug carrier, we used vitamin D3 as a model compound. The vitamin D3 concentration-dependence to the size, polydispersity, ζ-potential, encapsulation efficiency (EE(%)) and drug loading (DL(%)) were determined; the results are summarized in Table 1. Indicating successful encapsulation, both the polydispersity and the hydrodynamic diameter increase continuously from PDI ~ 0.152 and d_{DLS} ~ 240 (0 mg/mL D3) to PDI ~ 0.325 and d_{DLS} ~ 272 (0.1 mg/mL D3) with the amount of vitamin molecule. In contrast, systematic shift cannot be observed in the ζ-potential. EE(%) and DL(%) were studied by UV–Vis spectrophotometer. As Table 1 summarizes, the EE(%) has lower and lower value, so less active compound is encapsulated compared to the quantity added at baseline. However, opposite change is observed for the DL(%) and the highest value can be achieved at 0.10 mg/mL D3 (~22 %). In conclusion, the increase in the added amount of D3 to the carrier particles promotes the quantity of the encapsulated active substance, however the EE% is decreasing, which is costly from a financial point of view. To determine the effect of the HSA/HyA conjugates on the dissolution, we measured the release curve in case of 0.10 mg/mL D3-loaded HSA/HyA NPs, where bulk and dissolved vitamin were used as reference (Fig. 7).

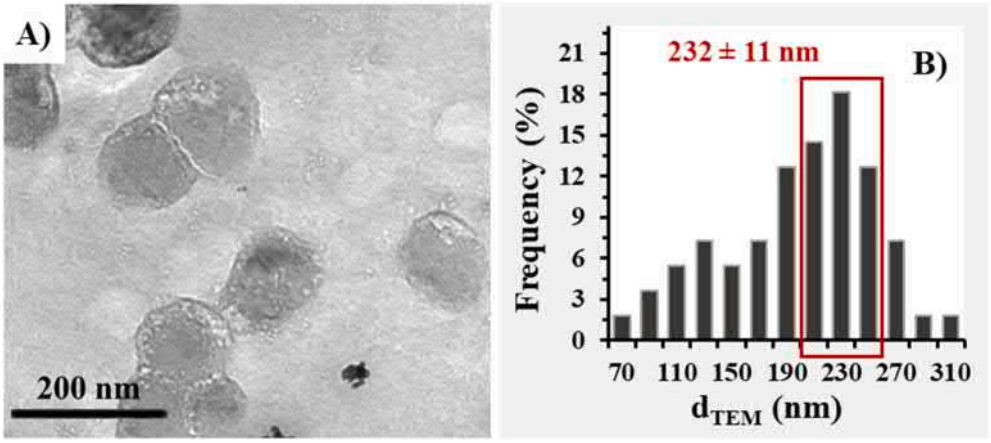

Fig. 5. (A) TEM image and (B) size distribution of the HSA/HyA particles.

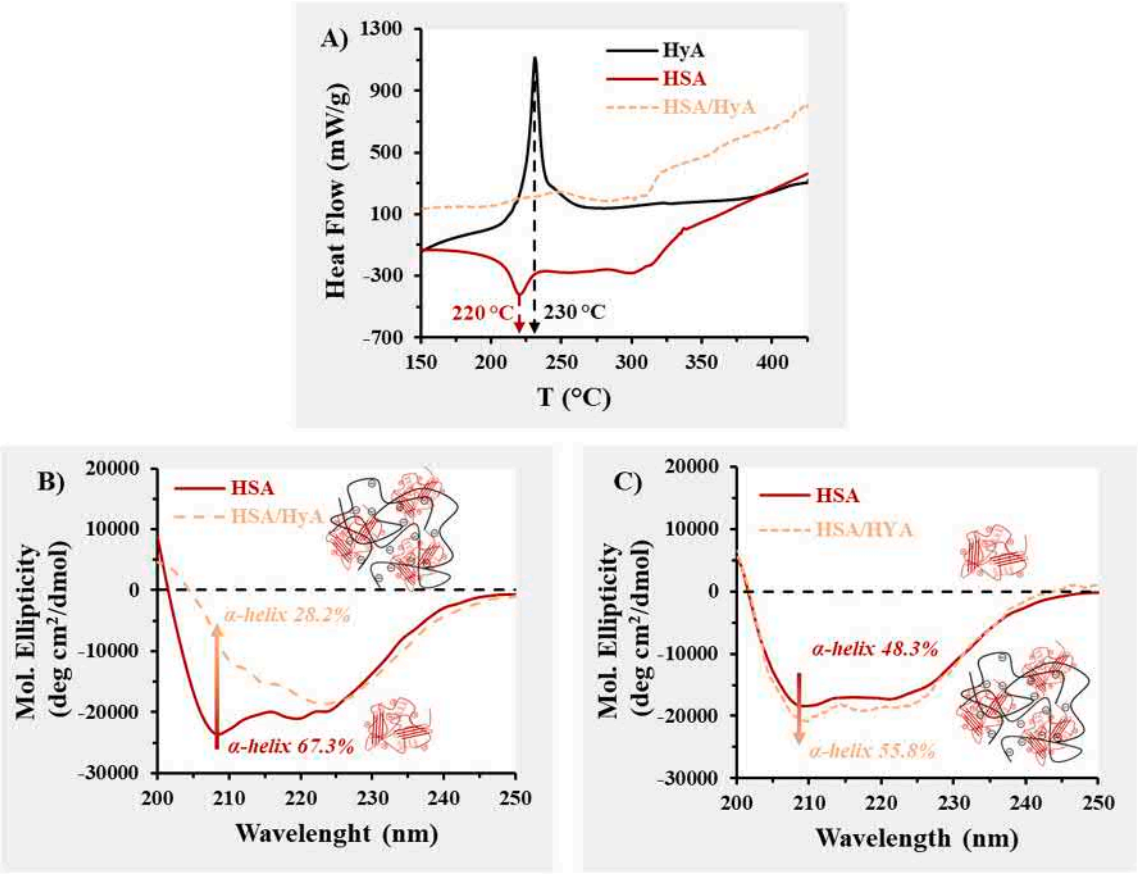

Fig. 6. (A) DSC curves of the HSA, HyA, and the lyophilized HSA/HyA conjugate, and CD curves of HSA (continuous red line) and HSA/HyA conjugates (dotted orange line) at $t = 25$ °C in (B) acetate buffer (pH = 4.5) and (C) phosphate buffer (pH = 7.4) ($c_{HSA} = 1.25$ μg/mL, $c_{HyA} = 0.625$ μg/mL). (For interpretation of the references to color in this figure legend, the reader is referred to the web version of this article.)

Table 1
Polydispersity index (*PDI*), hydrodynamic diameter (d_{DLS}), ζ-potential, encapsulation efficiency (*EE*) and drug loading (*DL*) of the HSA/HyA particles at different D3 concentration.

c_{D3} (mg/mL)	PDI ± SD	d_{DLS} ± SD (nm)	ζ ± SD (mV)	EE ± SD (%)	DL ± SD (%)
0.000	0.152 ± 0.091	240 ± 4	−38.5 ± 2.9	–	–
0.025	0.247 ± 0.101	250 ± 6	−31.9 ± 1.5	69 ± 5.3	10 ± 1.0
0.050	0.269 ± 0.032	265 ± 7	−30.7 ± 2.4	49 ± 2.1	14 ± 0.7
0.100	0.325 ± 0.075	272 ± 12	−35.4 ± 3.0	43 ± 3.1	22 ± 1.5

On the one hand, as expected, due to its extremely poor solubility, the penetration of the pure D3 molecules from their solution is much better than it was obtained for solid form, as Fig. 7 represents. When we analyze the dissolution of the D3 molecules for the carrier particles, it was obtained that faster dissolution process is occurred: $c_t/c_\infty = 10.0$ % for bulk D3 and $c_t/c_\infty = 20.1$ % for D3-loaded carriers in the 420 min time range. This can be explained, the application of nanosized conjugates with loose colloidal structure results larger specific surface area, thereby promoting the enhanced solubility and thus the possibility of higher D3 release. Further analyzing the dissolution curves, lower released drug concentration can be observed for the D3/HSA/HyA NPs than the D3 solution (57.0 % at 420 min), presumably due to retention of the drug in the carrier. The recorded dissolution data was fitted with different kinetic models (zero order, first order, Korsmeyer–Peppas, Peppas-Sahlin, Higuchi, Hixson and Weibull), but the first order, Korsmeyer-Peppas (Fig. 7B) and the Weibull (Fig. 7A) formulations give the best fit for the studied systems (Table 2). From the results, we conclude that the dissolution of drug from the carrier was mainly driven by diffusion effects, as we can see from the values from the Korsmeyer-Peppas model. Here, the diffusion dissolution index (n) exponent value is below 0.5, which represents full diffusion (Fickian) contribution, and zero relaxation effect (coming from matrix degradation, erosion or swelling). As the value is well below 0.5 ($n = 0.346$ for D3/HA/HyA NPs), we can assume that the carrier nanoparticles are spherical (in this case, the n value should be 0.42), and size distribution effects make the value even lower [29].

4. Conclusion

Considering the applicability as drug carrier, we performed the comprehensive characterization of the HSA/HyA macromolecule-based carrier particles. Summarizing the rheological and charge titration measurements, the interactions between the serum albumin and the polysaccharide are influenced by the applied HyA concentration. The results highlighted that the formation of the hydrophobic interaction can appear in addition to the electrostatic interaction. It was confirmed that the preparation of the electrostatically compensated HSA/HyA particles can be planned, which can be uniquely tuned with the initial synthesis parameter (*e.g.*, pH, dosing speed, temperature, HSA, HyA and inert salt concentrations). A production process has been optimized by controlling the size, size distribution and the ζ-potential that can be produced HSA/HyA conjugate with relatively small size and high stability ($d_{DLS} = 240 \pm 4$). The encapsulation and dissolution features of

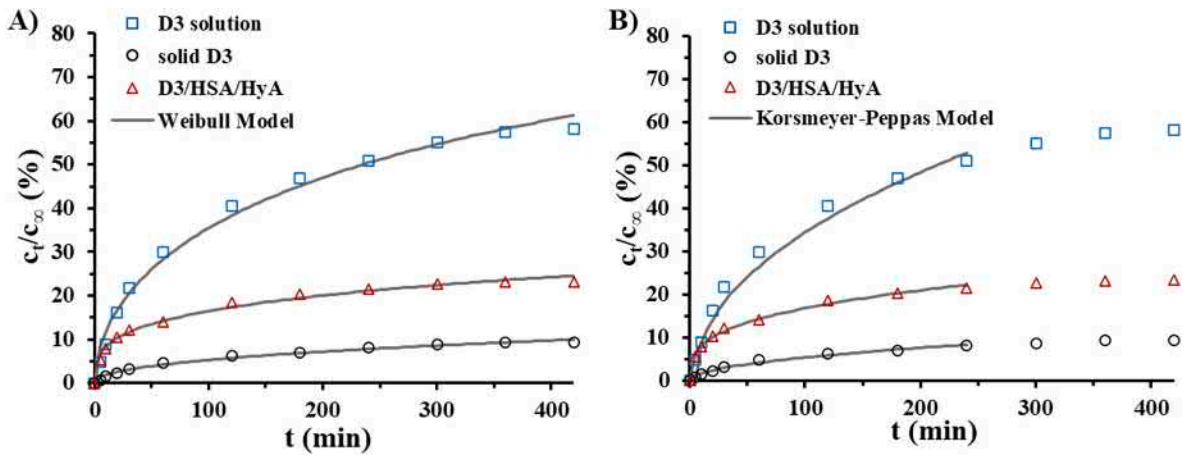

Fig. 7. Dissolution curves of the D3 in solid (○), dissolved (□) and encapsulated (△) form at 37 °C in PBS medium (pH = 7.4, 0.9 % NaCl, 0.5 % SDS). The solid lines show the fitting of the data by (A) Weibull- and (B) Korsmeyer-Peppas kinetic model. (For interpretation of the references to color in this figure legend, the reader is referred to the web version of this article.)

Table 2
Kinetic parameters of the fitted D3 dissolution curves using several kinetic models.

Formulation	First order		Weibull			Korsmeyer-Peppas		
	k (min^{-1})	R^2	a	b	R^2	k_m (min^{-n})	n	R^2
Solid D3	0.00810	0.9848	131.8	0.444	0.9878	0.00681	0.471	0.9855
D3 solution	0.00932	0.9910	29.1	0.544	0.9889	0.03579	0.492	0.9840
D3/HSA/HyA	0.01004	0.9774	32.1	0.328	0.9772	0.02988	0.346	0.9865

vitamin D3 as hydrophobic model compound were also studied. It was determined, even ~22 % drug loading (0.1 mg/mL D3) can be available by using this HSA/HyA nanoconjugate having hydrophilic character.

CRediT authorship contribution statement

Norbert Varga: Conceptualization, Writing – original draft, Writing – review & editing. **László Seres:** Methodology, Investigation, Visualization. **Nikolett Alexandra Kovács:** Methodology, Investigation. **Árpád Turcsányi:** Methodology, Investigation. **Ádám Juhász:** Validation, Formal analysis, Visualization. **Edit Csapó:** Conceptualization, Visualization, Writing – original draft, Writing – review & editing, Supervision, Resources.

Declaration of competing interest

The authors declare that they have no known competing financial interests or personal relationships that could have appeared to influence the work reported in this paper.

Data availability

Data will be made available on request.

Acknowledgement

This research was supported by the NRDIH through FK131446 project. E. Csapó thanks the financial support of the "Momentum" Program of the Hungarian Academy of Sciences (LP2021-5). Project no. TKP2021-EGA-32 has been implemented with the support provided by the Ministry of Innovation and Technology of Hungary from the National Research, Development and Innovation Fund. Á. Turcsányi thanks the support of NTP through NTP-NFTÖ-21-B-0069. The publication was also funded by the University of Szeged Open Access Fund (FundRef, Grant No. 5883).

Appendix A. Supplementary data

Supplementary data to this article can be found online at https://doi.org/10.1016/j.ijbiomac.2022.09.125.

References

[1] A. Kumari, S.K. Yadav, S.C. Yadav, Biodegradable polymeric nanoparticles based drug delivery systems, Colloids Surf. B: Biointerfaces 75 (2010) 1–18, https://doi.org/10.1016/J.COLSURFB.2009.09.001.
[2] Z. Liu, Y. Jiao, Y. Wang, C. Zhou, Z. Zhang, Polysaccharides-based nanoparticles as drug delivery systems, Adv. Drug Deliv. Rev. 60 (2008) 1650–1662, https://doi.org/10.1016/J.ADDR.2008.09.001.
[3] S. Sundar, J. Kundu, Subhas, C. Kundu, S.C. Kundu, Biopolymeric nanoparticles 11, 2010, https://doi.org/10.1088/1468-6996/11/1/014104.
[4] M. Bodnár, L. Daróczi, G. Batta, J. Bakó, J.F. Hartmann, J. Borbély, Preparation and characterization of cross-linked hyaluronan nanoparticles, <sb:contribution><sb:title>Colloid Polym.</sb:title></sb:contribution><sb:host><sb:issue><sb:series><sb:title>Sci.</sb:title></sb:series></sb:issue></sb:host> 287 (2009) 991–1000, https://doi.org/10.1007/S00396-009-2061-9/FIGURES/11.
[5] E. Csapó, H. Szokolai, Á. Juhász, N. Varga, L. Janovák, I. Dékány, Cross-linked and hydrophobized hyaluronic acid-based controlled drug release systems, Carbohydr. Polym. 195 (2018) 99–106, https://doi.org/10.1016/J.CARBPOL.2018.04.073.
[6] K. Bergman, C. Elvingson, J. Hilborn, G. Svensk, T. Bowden, Hyaluronic acid derivatives prepared in aqueous media by triazine-activated amidation, Biomacromolecules 8 (2007) 2190–2195, https://doi.org/10.1021/BM0701604/SUPPL_FILE/BM0701604SI20070420_111749.PDF.
[7] E.J. Kim, G. Shim, K. Kim, I.C. Kwon, Y.K. Oh, C.K. Shim, Hyaluronic acid complexed to biodegradable poly L-arginine for targeted delivery of siRNAs, J. Gene Med. 11 (2009) 791–803, https://doi.org/10.1002/JGM.1352.
[8] A.A.M. Gasperini, X.E. Puentes-Martinez, T.A. Balbino, T. de Paula Rigoletto, G. de Sá Cavalcanti Corrêa, A. Cassago, R.V. Portugal, L.G. de La Torre, L.P. Cavalcanti, Association between cationic liposomes and low molecular weight hyaluronic acid, Langmuir 31 (2015) 3308–3317, https://doi.org/10.1021/LA5045865/SUPPL_FILE/LA5045865_SI_001.PDF.
[9] N.V. Rao, J.G. Rho, W. Um, P.K. Ek, V.Q. Nguyen, B.H. Oh, W. Kim, J.H. Park, Hyaluronic acid nanoparticles as nanomedicine for treatment of inflammatory diseases, Pharmaceutics 2020 (12) (2020) 931, https://doi.org/10.3390/PHARMACEUTICS12100931.

[10] P. Sauerová, T. Pilgrová, M. Pekař, M.Hubálek Valbáčová, Hyaluronic acid in complexes with surfactants: the efficient tool for reduction of the cytotoxic effect of surfactants on human cell types, Int. J. Biol. Macromol. 103 (2017) 1276–1284, https://doi.org/10.1016/J.IJBIOMAC.2017.05.173.
[11] L. Yang, S. Gao, S. Asghar, G. Liu, J. Song, X. Wang, Q. Ping, C. Zhang, Y. Xiao, Hyaluronic acid/chitosan nanoparticles for delivery of curcuminoid and its in vitro evaluation in glioma cells, Int. J. Biol. Macromol. 72 (2015) 1391–1401, https://doi.org/10.1016/J.IJBIOMAC.2014.10.039.
[12] F.A. Oyarzun-Ampuero, F.M. Goycoolea, D. Torres, M.J. Alonso, A new drug nanocarrier consisting of polyarginine and hyaluronic acid, Eur. J. Pharm. Biopharm. 79 (2011) 54–57, https://doi.org/10.1016/J.EJPB.2011.04.008.
[13] R.R. Kudarha, K.K. Sawant, Hyaluronic acid conjugated albumin nanoparticles for efficient receptor mediated brain targeted delivery of temozolomide, J.Drug Deliv. Sci.Technol. 61 (2021), 102129, https://doi.org/10.1016/J.JDDST.2020.102129.
[14] Z. Chen, J. Chen, L. Wu, W. Li, J. Chen, H. Cheng, J. Pan, B. Cai, Hyaluronic acid-coated bovine serum albumin nanoparticles loaded with brucine as selective nanovectors for intra-articular injection, Int. J. Nanomedicine 8 (2013) 3843, https://doi.org/10.2147/IJN.S50721.
[15] F. Zeeshan, T. Madheswaran, J. Panneerselvam, R. Taliyan, P. Kesharwani, Human serum albumin as multifunctional nanocarrier for cancer therapy, J. Pharm. Sci. 110 (2021) 3111–3117, https://doi.org/10.1016/J.XPHS.2021.05.001.
[16] E. Miele, G.P. Spinelli, E. Miele, F. Tomao, S. Tomao, Albumin-bound formulation of paclitaxel (Abraxane® ABI-007) in the treatment of breast cancer, Int. J. Nanomedicine 4 (2009) 99, https://doi.org/10.2147/IJN.S3061.
[17] T. Saleh, T. Soudi, S.A. Shojaosadati, Redox responsive curcumin-loaded human serum albumin nanoparticles: preparation, characterization and in vitro evaluation, Int. J. Biol. Macromol. 114 (2018) 759–766, https://doi.org/10.1016/J.IJBIOMAC.2018.03.085.
[18] P. Rahimizadeh, S. Yang, S.I. Lim, Albumin: an emerging opportunity in drug delivery, Biotechnol. Bioprocess Eng. 2020 (25) (2020) 985–995, https://doi.org/10.1007/S12257-019-0512-9.
[19] D. Huang, Y.S. Chen, C.R. Green, I.D. Rupenthal, Hyaluronic acid coated albumin nanoparticles for targeted peptide delivery in the treatment of retinal ischaemia, Biomaterials 168 (2018) 10–23, https://doi.org/10.1016/J.BIOMATERIALS.2018.03.034.
[20] Y. Shen, W. Li, HA/HSA co-modified erlotinib–albumin nanoparticles for lung cancer treatment, Drug Des.Dev.Ther. 12 (2018) 2285, https://doi.org/10.2147/DDDT.S169734.
[21] T. del Castillo-Santaella, A. Aguilera-Garrido, F. Galisteo-González, M.J. Gálvez-Ruiz, J.A. Molina-Bolívar, J. Maldonado-Valderrama, Hyaluronic acid and human/bovine serum albumin shelled nanocapsules: interaction with mucins and in vitro digestibility of interfacial films, Food Chem. 383 (2022), 132330, https://doi.org/10.1016/J.FOODCHEM.2022.132330.
[22] M. Tarhini, H. Greige-Gerges, A. Elaissari, Protein-based nanoparticles: from preparation to encapsulation of active molecules, Int. J. Pharm. 522 (2017) 172–197, https://doi.org/10.1016/J.IJPHARM.2017.01.067.
[23] Á. Turcsányi, N. Varga, E. Csapó, Chitosan-modified hyaluronic acid-based nanosized drug carriers, Int. J. Biol. Macromol. 148 (2020) 218–225, https://doi.org/10.1016/J.IJBIOMAC.2020.01.118.
[24] A.N. Kovács, N. Varga, Á. Juhász, E. Csapó, Serum protein-hyaluronic acid complex nanocarriers: structural characterisation and encapsulation possibilities, Carbohydr. Polym. 251 (2021), 117047, https://doi.org/10.1016/J.CARBPOL.2020.117047.
[25] A.N. Kovács, G. Katona, Á. Juhász, G.T. Balogh, E. Csapó, Albumin-hyaluronic acid colloidal nanocarriers: effect of human and bovine serum albumin for intestinal ibuprofen release enhancement, J. Mol. Liq. 351 (2022), 118614, https://doi.org/10.1016/J.MOLLIQ.2022.118614.
[26] D.P. Fonseca, N.M. Khalil, R.M. Mainardes, Bovine serum albumin-based nanoparticles containing resveratrol: characterization and antioxidant activity, J. Drug Deliv.Sci.Technol. 39 (2017) 147–155, https://doi.org/10.1016/J.JDDST.2017.03.017.
[27] J. Wang, B. Zhang, Bovine serum albumin as a versatile platform for cancer imaging and therapy, Curr. Med. Chem. 25 (2017) 2938–2953, https://doi.org/10.2174/0929867324666170314143335.
[28] Y. Zhao, T. Xin, T. Ye, X. Yang, W. Pan, Solid dispersion in the development of a nimodipine delayed-release tablet formulation, Asian J.Pharm.Sci. 9 (2014) 35–41, https://doi.org/10.1016/J.AJPS.2013.11.006.
[29] N. Varga, Á. Turcsányi, V. Hornok, E. Csapó, Vitamin E-loaded PLA- and PLGA-based Core-Shell nanoparticles: synthesis,structure optimization and controlled drug release, Pharmaceutics 2019 (11) (2019) 357, https://doi.org/10.3390/PHARMACEUTICS11070357.
[30] L. Janovák, Á. Turcsányi, É. Bozó, Á. Deák, L. Mérai, D. Sebők, Á. Juhász, E. Csapó, M.M. Abdelghafour, E. Farkas, I. Dékány, F. Bari, Preparation of novel tissue acidosis-responsive chitosan drug nanoparticles: characterization and in vitro release properties of Ca2+ channel blocker nimodipine drug molecules, Eur. J. Pharm. Sci. 123 (2018) 79–88, https://doi.org/10.1016/J.EJPS.2018.07.031.
[31] H.M. Wang, D. Loganathan, R.J. Linhardt, Determination of the pKa of glucuronic acid and the carboxy groups of heparin by 13C-nuclear-magnetic-resonance spectroscopy, Biochem. J. 278 (1991) 689–695, https://doi.org/10.1042/BJ2780689.
[32] R.J. Sarmah, S. Kundu, Structure, morphology and reversible hysteresis nature of human serum albumin (HSA) monolayer on water surface, Int. J. Biol. Macromol. 174 (2021) 377–384, https://doi.org/10.1016/J.IJBIOMAC.2021.01.131.
[33] R. Yan, P. DeLos Ríos, A. Pastore, P.A. Temussi, The cold denaturation of IscU highlights structure–function dualism in marginally stable proteins, <sb:contribution><sb:title>Commun. </sb:title></sb:contribution><sb:host><sb:issue><sb:series><sb:title>Chem.</sb:title></sb:series></sb:issue></sb:host> 1 (2018) (2018) 1–7, https://doi.org/10.1038/s42004-018-0015-1.
[34] J. Reed, T.A. Reed, A set of constructed type spectra for the practical estimation of peptide secondary structure from circular dichroism, Anal. Biochem. 254 (1997) 36–40, https://doi.org/10.1006/ABIO.1997.2355.